Space Sci Rev (2010) 153: 273–298
DOI 10.1007/s11214-009-9619-1

Rheological and Thermal Properties of Icy Materials

W.B. Durham · O. Prieto-Ballesteros · D.L. Goldsby · J.S. Kargel

Received: 26 May 2009 / Accepted: 1 December 2009 / Published online: 20 February 2010

Abstract Laboratory measurements of physical properties of planetary ices generate information for dynamical models of tectonically active icy bodies in the outer solar system. We review the methods for measuring both flow properties and thermal properties of icy planetary materials in the laboratory, and describe physical theories that are essential for intelligent extrapolation of data from laboratory to planetary conditions. This review is structured with a separate and independent section for each of the two sets of physical properties, rheological and thermal. The rheological behaviors of planetary ices are as diverse as the icy moons themselves. High-pressure water ice phases show respective viscosities that vary over four orders of magnitude. Ices of CO_2, NH_3, as well as clathrate hydrates of CH_4 and other gases vary in viscosity by nearly ten orders of magnitude. Heat capacity and thermal conductivity of detected/inferred compositions in outer solar system bodies have been revised. Some low-temperature phases of minerals and condensates have a deviant thermal behavior related to paramount water ice. Hydrated salts have low values of thermal conductivity and an inverse dependence of conductivity on temperature, similar to clathrate hydrates or glassy solids. This striking behavior may suit the dynamics of icy satellites.

Keywords Thermal properties · Heat capacity · Thermal conductivity · Cryomagmatism · Thermal gradient · Rheology · Flow strength · Grain size · Grain boundary sliding

W.B. Durham (✉)
Massachusetts Institute of Technology, Cambridge, MA 02127, USA
e-mail: wbdurham@mit.edu

O. Prieto-Ballesteros
Centro de Astrobiología-INTA-CSIC, Ctra. Ajalvir km. 4, 28850 Torrejón de Ardoz, Spain
e-mail: prietobo@inta.es

D.L. Goldsby
Brown University, Providence, RI 02912, USA
e-mail: David_Goldsby@brown.edu

J.S. Kargel
Department of Hydrology, University of Arizona, Tucson, AZ 85721, USA
e-mail: jkargel1054@earthlink.net

1 Introduction to Rheological Properties

The rheology of water ice and other frozen volatiles has primary influence on the evolution and appearance of low-density moons in the outer solar system. The diverse kinds of past and present activity on these moons is driven by internal and external energy sources (radiogenic, gravitational, tidal), and includes planetary-scale convection to smaller-scale relaxation of surface topography. Internally, if ice flows readily, the moon is efficiently cooled; if ice resists flow, in the extreme the moon will overheat, begin to melt internally, and differentiate catastrophically. Warm ice flowing in the subsurface exerts tractions on a cold icy crust, which, if sufficient to overcome the strength of the crust, may cause the crust to fail. On an icy crust, impact craters and other landforms relax under gravitational forces at a rate controlled by the viscosity of ice.

The flow and fracture of water ice under terrestrial conditions has seen extensive study, and a great body of literature exists describing its rheological properties. The "Glen law" for the creep of polycrystalline ice, relating strain rate to the third power of shear stress, owes its origins to one of the first systematic laboratory studies of ice flow (Glen 1952, 1955). The Glen law is still the rule of thumb for glaciologists, although the implications for glaciology of the new rheological descriptions for ice flow described below are being explored. Most of the ice in planetary environments is mostly either much colder or exists at far higher pressures than on Earth, and flow under these conditions may differ significantly from terrestrial ice flow. Laboratory experiments undertaken in support of planetary exploration have begun to provide a catalog of rheological characterizations applicable to models of planetary dynamics and evolution and to the dynamics of terrestrial glaciers and ice sheets. Here we provide a survey of those experiments and measurements as well as a brief introduction to our current understanding of the physics of deformation in planetary settings.

1.1 The Flow Law

Rheology is the study of deformation of materials. The fundamental rheological relationship can be written as

$$\dot{\varepsilon} = A' f(\sigma), \tag{1}$$

where $\dot{\varepsilon}$ and σ are, respectively, strain rate and an appropriate scalar representation of the state of deviatoric stress (differential stress or octahedral shear stress, for example). The factor A' comprises the effect of all relevant environmental conditions on the relationship between $\dot{\varepsilon}$ and σ. Relationship (1) describes flow, and so implicitly applies to large strain or "steady state" deformation that does not vary with strain. The term "viscosity" refers generally to the ratio of $\sigma/\dot{\varepsilon}$. There are important aspects of the strength of materials that have relevance to near-surface geologic and planetary settings: transient deformation at low absolute strains, brittle faulting, and shock deformation during impact. We limit our discussion here to steady-state ductile flow.

Most of the steady-state flow of planetary ices encountered in laboratory experiments and that presumably exists in planetary settings can be described using a power-law form of the flow law:

$$\dot{\varepsilon} = A d^{-p} \sigma^n \exp\left(-\frac{E^* + PV^*}{RT}\right) \tag{2}$$

where we now make explicit the environmental variables: grain size d, hydrostatic pressure (i.e., mean stress) P, and temperature T; and the material-specific parameters: grain size

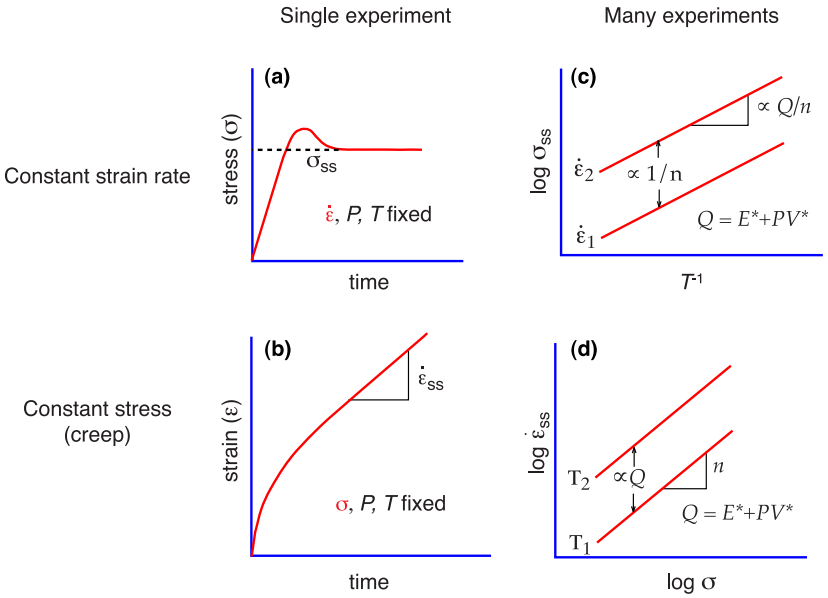

Fig. 1 The two basic laboratory approaches to measuring the parameters in (2): (**a**) Measure the stress required to hold a constant strain rate, or (**b**) measure the strain rate that results from the application of constant stress; (**c**) and (**d**), results from many experiments plotted as a locus of points can be used to solve graphically for material constants

exponent p, stress exponent n, activation energy E^*, and activation volume V^*, along with the pre-exponential constant A comprising all dependencies that have not yet been identified. The functional form of the temperature and pressure dependence will be recognized as that describing a thermally activated process.

1.2 Laboratory Measurement of Rheological Properties

An axisymmetric geometry is one of the practical designs for our mechanical testing instruments because of the necessity in some cases (for example, for relatively large-grained samples) to apply high hydrostatic confinement to samples in order to suppress fracturing and remain in the more planetarily relevant ductile field of deformation.[1] Samples are thus often cylindrical in shape, and deformation is induced by applying a load to the end of the sample with a moving piston, usually in compression. In this condition, the stress term in (2) becomes the differential stress, i.e., the difference between the maximum stress σ_1 applied to the ends of the sample and the gas pressure applied to the outside of the sample. The strain rate is obtained from the rate of shortening of the cylinder.

We approach rheological measurements in either of two ways suggested by the flow law. In a so-called "constant displacement rate" experiment we impose a strain rate with the deforming piston and measure as the dependent variable the stress (load divided by cross-sectional area of the sample) required to maintain that rate (Fig. 1a). Alternatively, in a

[1]The application of hydrostatic pressure during deformation is required to suppress fracturing of coarse-grained polycrystals, e.g., $d > 1$ mm at stresses $\sigma > 1$ MPa for ice, since the fracture strength is inversely proportional to $d^{1/2}$. The need to apply hydrostatic pressure can thus be negated by using fine-grained samples.

constant stress or "creep" experiment, we prescribe the load and measure the displacement rate required to maintain that load (Fig. 1b). Among the many ways of presenting results graphically, there are two styles employed in this paper: the Arrhenius plot of $\log\sigma$ vs. inverse temperature (Fig. 1c), which is convenient for displaying the results of constant strain rate experiments, and $\log\dot{\varepsilon}$ vs. $\log\sigma$ (Fig. 1d). Activation energies and stress exponents, respectively, can be identified graphically on such plots as shown in Fig. 1, c and d.

2 Mechanisms of Creep

In broad terms, the steady-state flow of materials is controlled by grain size-insensitive (GSI) dislocation mechanisms (low-temperature plasticity and power-law creep) at high stresses, and grain size-sensitive (GSS) mechanisms involving grain boundary sliding (GBS) at lower stresses (Frost and Ashby 1982). At the highest stresses, typically achieved at low temperatures in the laboratory, the creep rate is limited by the lattice resistance to the glide of dislocations and is characterized by relatively weak dependences of flow stress on strain rate and temperature; in the limit of 'perfect plasticity,' the flow stress is independent of deformation rate. At lower stresses, typically associated with higher temperatures in the laboratory, "power-law creep" (or dislocation creep) occurs via either the glide of dislocations or via the combined glide and climb of dislocations. Dislocation creep is characterized by a power-law dependence of creep rate on stress and an exponential dependence of creep rate on temperature (e.g., see (2)). In cases where glide and climb occur simultaneously as serial mechanical processes, the creep rate is often limited by dislocation climb. At the lowest stresses and at high temperatures, various GSS creep mechanisms become dominant over dislocation creep. The creep rate for these low-stress mechanisms increases strongly with decreasing grain size, so that these mechanisms become accessible at practical strain rates in the laboratory by deforming samples of very fine grain size. Such creep mechanisms can dominate the flow of materials in low-differential-stress planetary environments, for example, in flow of ice in polar ice caps (Nye 2000; Nye et al. 2000), in 'viscous flow features' (Milliken et al. 2003) on Mars, and in the interiors of the icy satellites (Dombard and McKinnon 1996, 2000; Pappalardo et al. 1998; Nimmo and Manga 2002). These same mechanisms likely control the flow of ice under most conditions that occur within terrestrial glaciers and ice sheets (Goldsby and Kohlstedt 2001; Goldsby 2006). Here we focus on the creep mechanisms most relevant for planetary flow of ice, dislocation creep and the various GSS mechanisms.

2.1 Grain Size-Insensitive Creep

Power-law creep or dislocation creep occurs via the motion of lattice dislocations. When a stress of sufficient magnitude is applied to a polycrystalline sample, grains within the sample that are well oriented for slip deform via dislocation glide. These gliding dislocations may encounter other dislocations, or dislocation structures (e.g., tilt walls, dislocation pile-ups, dislocation tangles) which impede their motion. For steady-state deformation to occur, dislocations must 'climb,' allowing for blocked dislocations to glide on their glide planes. Dislocation creep can be either 'glide-limited,' i.e., limited by the glide of lattice dislocations, or 'climb-limited,' i.e., limited by the climb of lattice dislocations, depending on which is the slower process. When climb is rate limiting, the activation energy for creep is equivalent to that for volume diffusion. Typical values of the stress exponent for dislocation creep are $n = 3{-}5$, and dislocation creep is often independent of grain size. Dislocation

creep requires five independent deformation systems (e.g., glide, climb) for homogeneous deformation on the grain scale, or possibly fewer if locally heterogeneous deformation is allowed (see, e.g., Paterson 1969).

2.2 Grain Size-Sensitive Creep

2.2.1 Grain Boundary Sliding

At low stresses, deformation mechanisms involving GBS control the creep rate of materials. However, it must be emphasized that GBS cannot occur in isolation, i.e., it is not an independent creep mechanism. Upon application of a stress to a polycrystalline sample, sliding occurs along grain boundaries, inducing a stress concentration at triple junctions. For small strains, GBS is accommodated by elastic deformation of the material at triple junctions. To achieve larger strains (as during steady-state creep), i.e., to deform the material in a volume-conservative fashion without cavitation or microfracturing, GBS must be accommodated by transfer of material away from the stress concentrations induced by sliding. During steady-state flow, GBS is accommodated by either diffusional flow of material or dislocation flow of material.

2.2.2 Diffusion-Accommodated GBS (Diffusion Creep)

In the so-called diffusion creep regime, GBS and diffusional flow are mutually accommodating creep processes that allow grain-scale stress concentrations induced by GBS to relax (Raj and Ashby 1971), allowing for steady-state deformation. The diffusional flow of material away from and the counterflux of vacancies toward areas of stress concentration occur within grain interiors or along grain boundaries, with the creep rate limited by the faster of these two diffusion steps. First-principles derivations of the diffusion creep equation (Nabarro 1948; Herring 1950; Coble 1963) predict a linear dependence of creep rate on stress for both volume diffusion creep ("Nabarro–Herring creep") and grain boundary diffusion creep ("Coble creep"), with grain size dependences of $p = 2$ and 3, respectively, and activation energies equivalent to those for volume diffusion and grain boundary diffusion, respectively. The diffusion creep equation is given in general form by

$$\dot{\varepsilon} = \frac{42\sigma}{3RT}\left[\frac{D_v}{d^2} + \frac{\pi\delta D_b}{d^3}\right] \tag{3}$$

where δ is the grain boundary width, and D_v and D_b are diffusion coefficients for volume and grain boundary diffusion, respectively, each of the form

$$D_i = D_0 \exp\left(\frac{-Q_i}{RT}\right) \tag{4}$$

where Q is the activation energy and the subscript i indicates v or b. Experiments on a wide range of materials have corroborated these theoretical predictions (Burton 1977); diffusion creep data for ice, however, are lacking (see below).

2.2.3 Dislocation-Accommodated GBS ('Superplastic Flow')

Grain boundary sliding during steady-state creep can also be accommodated by the motion of lattice dislocations. Such behavior is thought to underlie so-called "superplasticity,"

the phenomenological behavior whereby materials can be deformed to large strains in tension, sometimes to spectacular strains of thousands of percent, without necking and failure. Although considerable controversy exists as to the precise physical mechanism underlying superplasticity, many workers have emphasized the importance of intragranular dislocation slip as well as GBS during superplastic flow (e.g., Ball and Hutchinson 1969; Langdon 1970; Mukherjee 1971; Gifkins 1976; Kaibyshev 1992). Values of flow law parameters n, p and Q ($= E^* + PV^*$) in (2) obtained from experiments on materials deformed in the superplastic flow regime (Region II in the superplasticity parlance) vary somewhat, but values of $n = 2$, $p = 2$, and $Q = Q_b$ are typical. Hence, models of superplastic flow typically yield values of $n = 2$, $p = 2$, and $Q = Q_b$.

The rheological behavior of water ice—Within the past decade, critical advances have been made in understanding the rheological behavior of water ice (ice I and to a lesser extent ice II) relevant to flow in low-differential-stress planetary environments (Goldsby et al. 1993; Goldsby and Kohlstedt 1995, 1997a, 1997b, 2001; Stern et al. 1997; Durham et al. 2001; Kubo et al. 2006). These discoveries were made possible in large part by the development of novel methods for fabricating ice samples of exceedingly fine grain size (<200 μm), which allow for exploration of grain size-sensitive creep mechanisms like diffusion creep and superplastic flow, as well as dislocation creep, at practical laboratory strain rates ($>1 \times 10^{-8}$ s^{-1}).

3 Rheological Behavior of Planetary Ices

3.1 Dislocation Creep of Planetary Ices

3.1.1 Water Ices I and High-Pressure Phases

Flow of ice in the power-law creep regime is classically described by the Glen flow law, which holds that stress exponent $n = 3$ in (2). In spite of the widespread adoption of the Glen law in the terrestrial glaciological community, more recent laboratory experiments on relatively coarse-grained ice samples consistently yield a stress exponent of $n \approx 4$ at differential stresses >1 MPa (e.g., Durham et al. 1997). Higher-stress data in the power-law creep regime are also in excellent agreement with relatively high-stress creep data on fine-grained samples (Goldsby and Kohlstedt 2001; Durham et al. 2001), demonstrating the grain size insensitivity of this mechanism. Although Glen law flow of ice in the power-law creep regime has been most often attributed to a dislocation glide mechanism (e.g., Frost and Ashby 1982), the equivalence of the value of the activation energy for dislocation creep with that for volume diffusion (Ramseier 1967a, 1967b), ~60 kJ/mol, and the good agreement of the value of $n = 4$ in the dislocation creep regime with theoretical models of climb-limited dislocation creep (e.g., Weertman 1968) suggest that dislocation creep of ice may be limited by dislocation climb.

Dislocation creep laws for ice I as well as for high-pressure phases II, III, V, and VI are illustrated in Fig. 2. The broad field associated with ice I is described with a rheology of $n = 4$, $E^* = 60$ kJ/mol and $V^* = -11$ m^3/mol (i.e., ice I becomes *weaker* at higher pressure). This regime applies to a temperature range of roughly 150–250 K at planetary strain rates (see, e.g., the curve labeled 3.5×10^{-14} s^{-1} in Fig. 2). The flow law constants associated with this lower-temperature regime can be expected to apply to most planetary conditions in those cases when the ice is deforming via dislocation creep. An important exception is at the base of an ice shell overlying an internal ocean where the water in that ocean is sufficiently

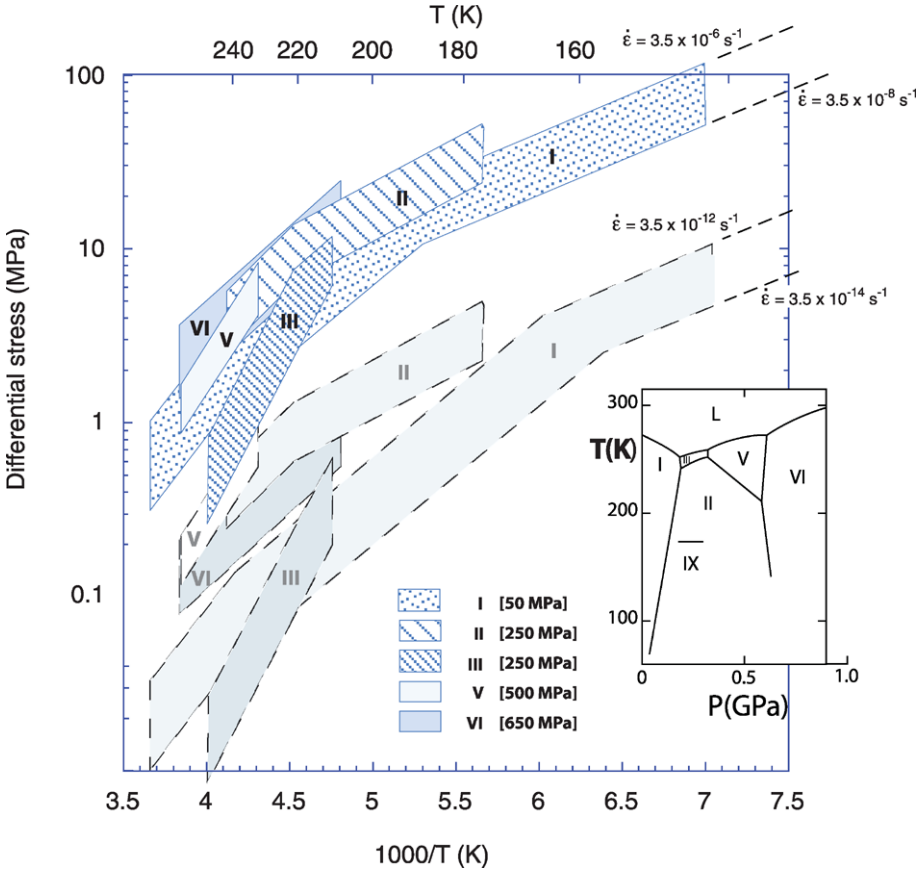

Fig. 2 Arrhenius plot (see Fig. 1(c)) of flow stress for several phases of ice I at fixed strain rate. *Inset* phase diagram shows the equilibrium locations of the several phases in T, P space. *Numbers in brackets in the legend* give the hydrostatic pressure. Fields (labeled by phase) in the Arrhenius plot are bounded by locations of phase transformations (except for the right hand boundaries for ices I, II, and VI) and on the top and bottom by the locus of differential stress values at two strain rates (see labels on the ice I field) two orders of magnitude apart. The top set of fields are directly measured at lab strain rates; the ghosted bottom set of fields are extrapolated to planetary rates using (2). Higher differential stress at a given strain rate means higher viscosity. It can be seen that ices II and VI are the strongest phases at lab rates, but the slightly lower stress sensitivity of ice II means that at lower planetary rates, ice II becomes stronger than ice VI. Ice III is the weakest phase at all strain rates, with ice I being the next weakest

pure that its melting temperature is above 250 K. In that case, the apparent temperature sensitivity of flow will be higher, $E^* \geq 90$ kJ/mol. The flow of ice at warm conditions has obvious terrestrial applications and is for the most part beyond the "planetary" scope of the present paper. Many excellent reviews of the flow of ice in terrestrial settings are available (Alley 1992; Budd and Jacka 1989; Paterson 1994; Petrenko and Whitworth 1999; Schulson and Duval 2009).

The several phases of water ice are rheologically distinct (Fig. 2). It can also be seen in Fig. 2 that relative viscosities of the ice phases in the dislocation creep regime are different at laboratory strain rates (of order 10^{-6} s^{-1}) than they are at planetary rates ($<10^{-12}$ s^{-1}), as extrapolated based on (2). (As discussed below, different creep mechanisms appearing at

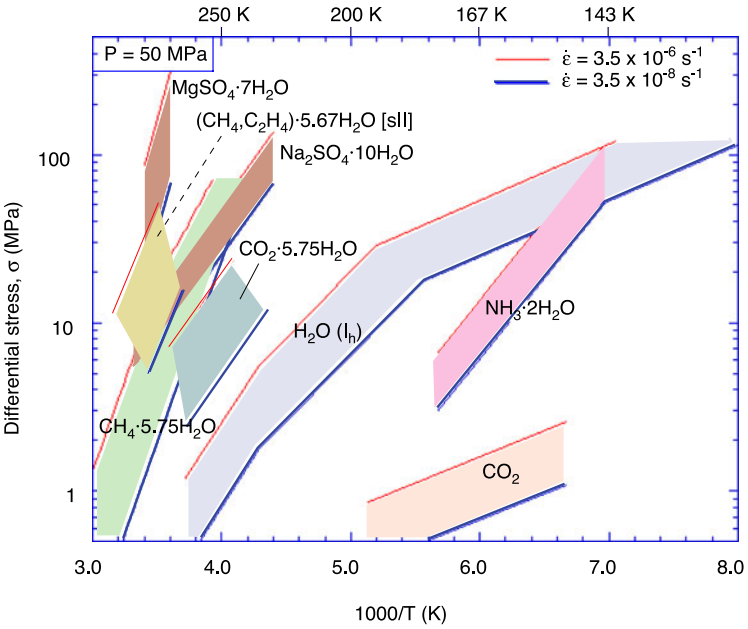

Fig. 3 Steady-state rheological behavior of several planetary ices and mixtures, for grain size-insensitive mechanisms ($p = 0$ in (2)). In approximate order of increasing viscosity are dry ice, ammonia dihydrate, water ice, CO_2 clathrate, methane (CH_4) clathrate, mirabilite ($Na_2SO_4 \cdot 10H_2O$), structure II methane-ethane clathrate, and epsomite ($MgSO_4 \cdot 7H_2O$). Top and bottom boundaries for each field are loci of constant strain rate that are two orders of magnitude apart. Plot is Arrhenius-style (as in Fig. 1(c)), so stress exponent n can be immediately seen as inversely proportional to vertical distance between lines of constant strain rate, and Q/n proportional to the slope of those lines

low stress may change these relationships in the planetary setting.) Each field in Fig. 2 is bounded by fixed strain rates that are two orders of magnitude apart. Perhaps the strongest viscosity contrast is that along the ice I–III boundary, roughly two orders of magnitude at both laboratory and planetary strain rates, and along the ice II–III boundary, where the contrast is roughly 6 orders of magnitude at planetary rates. Given that ice III displays such profound weakness, it is likely that the II–III boundary is an attractor for temperature-depth profiles, meaning that the layer beneath an ice I layer would be comprised of mixed ice II+III. If this is not the case, then the horizontal viscosity layering between I and the much weaker (III) or much stronger (II) phase will likely disrupt large-scale convection.

Figure 2 applies strictly to the behavior of GSI creep mechanisms. GSS creep in ice I has been intensively studied by two research groups, and in ice II by one group. Those results are discussed in the GSS creep section below.

3.1.2 Comparative Rheology of Other Icy Materials

In contrast to ice I, whose rheological behavior and deformation physics has been studied with rigor, other ices of interest in planetology have been the subject of only cursory lab research of their behavior under stress. Most of that research has been conducted since images from the Voyager spacecraft in the late 1970s revealed that icy moons had stunningly varied and active dynamic histories.

Figure 3 is an Arrhenius plot comparing the rheological behaviors of the more common ices that are proven or anticipated building materials of the icy moons of the outer solar system, and of the near surface of Mars. The measurements have been carried out for the most part in the laboratory of one of the authors (WBD), and Fig. 3 is compiled from studies carried out over a wide interval of time (Durham et al. 1983, 1993, 1999, 2003, 2005a, 2005b). In the absence of detailed microscopy or studies of the effect of grain size on creep for most of these materials, we take the behavior to be dislocation creep, and the curves in Fig. 2 are fit to (2) with the parameter $p = 0$, i.e. with GSS processes assumed insignificant. The various curves in Fig. 2 in fact all show $n \geq 3$ (see (2)), so the assumption of dislocation creep is apparently borne out.

The shaded fields in Fig. 3 are defined as in Fig. 2. They apply to laboratory strain rates, and generally reflect directly measured (i.e., not extrapolated) values. For reference, the ice I field from Fig. 2 is reproduced in Fig. 3. Again using a viscosity contrast scale that is two orders of magnitude vertically across any field, it is obvious that the range of viscosities of planetary ices is huge, far larger, say, than the contrasts among water ice phases (Fig. 2). Keeping in mind the composition of Earth's crust and mantle, we should expect that many of these phases are likely to be mixed in planetary environments. The rheological implications of mixing phases of different viscosities can be very complex, and are discussed near the end of this section. A mixture of dry ice (CO_2) and ice I will obviously involve very little deformation of the ice I phase given the >6 order-of-magnitude viscosity contrast between the two phases, except for very ice-rich compositions. Given the extremely low viscosity of dry ice, and knowledge of the age and shape of the Martian South Polar Cap, for example, Nye et al. (2000) concluded that the cap contains very little dry ice in its interior. Clathrate hydrates on the other hand are essentially undeformable compared with ice I, so significant concentrations of clathrates in ice I layers will be significant obstacles to deformation of that layer. Likewise, hydrated sulfate salts such as may exist in the Europan ice shell, technically not ices but appearing in Fig. 3 nonetheless, cannot actively deform with ice I.

3.2 Dislocation-Accommodated GBS in Ice I

With decreasing stress, for ice I samples of sufficiently small grain size (<200 μm), a transition occurs from dislocation creep, with $n = 4$, to a creep mechanism characterized by $n = 1.8$, as shown schematically in Fig. 4. The creep rate in this regime increases systematically with decreasing grain size, yielding a grain size exponent of $p = 1.4$. The value of the activation energy in this creep regime is ~49 kJ/mol, ~0.8 times that of the activation energy for volume diffusion. These values of the flow law parameters are consistent with various models of dislocation-accommodated GBS, constructed in part to explain observations of 'superplastic flow' (e.g., Ball and Hutchinson 1969; Langdon 1970; Mukherjee 1971; Gifkins 1976; Kaibyshev 1992). In addition to these mechanical data, microstructural observations of samples deformed within this creep regime to large strains of up to 0.8 reveal a lack of significant grain flattening and ubiquitous 4-grain junctions (Goldsby and Kohlstedt 1997a, 1997b), both of which have been described as indicators of GBS and grain-switching events during superplastic flow (e.g., Ashby and Verrall 1973).

With further decreasing stress, a transition occurs from a stress exponent of $n = 1.8$ to $n = 2.4$. In addition, the activation energy changes from $Q = 49$ kJ/mol in the $n = 1.8$ regime to $Q = 60$ kJ/mol in the $n = 2.4$ regime. The creep data for polycrystalline samples in this regime are in excellent agreement with data for single crystals of ice oriented for optimal slip on the basal dislocation slip plane (e.g., Wakahama 1967). The creep rate (or flow stress) of ice within this $n = 2.4$ regime is independent of grain size.

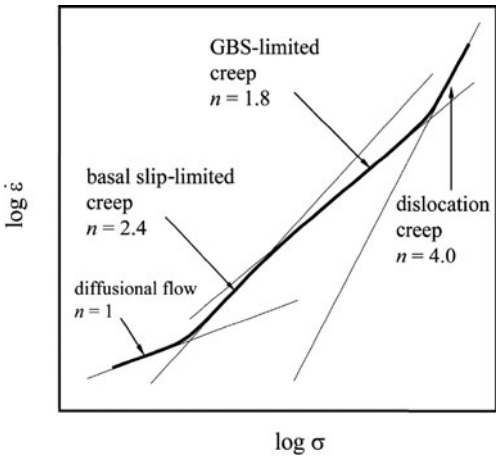

Fig. 4 Schematic diagram showing the various creep regimes for ice I (from Goldsby and Kohlstedt 2001)

3.3 Diffusion-Accommodated GBS in Ice I

Diffusion-accommodated GBS (i.e., diffusion creep) is anticipated to occur at lower stresses than for dislocation-accommodated GBS (e.g., Mukherjee 1971); however, no experimental data for diffusion creep yet exist for ice. There is, however, no reason to doubt its existence (Duval et al. 1983). The question for experimentalists is: can we devise experiments to access the diffusion creep regime of ice in the laboratory?

3.4 A New Rheological Model for Ice I

The rheological behavior described above suggests the following interpretation of experimental (and anticipated, for the case of diffusion creep) data represented schematically in Fig. 4: At sufficiently high stresses, ice samples deform via dislocation creep which is characterized by $n = 4$. Dislocation glide in ice occurs most easily on the basal plane, and with increasing difficulty on the prismatic and pyramidal slip systems. Dislocation creep requires activation of dislocations on both the basal slip system and harder, non-basal slip systems, such that the creep strength at a given strain rate is an appropriate average of easy and hard slip systems.

With decreasing stress, the rate of GBS becomes sufficiently fast, so that compatible deformation can occur via dislocation slip on the basal plane acting in concert with GBS. The effect of GBS is to ease compatibility requirements and effectively 'lose' the hard slip systems required for deformation in the dislocation creep regime, allowing for compatible deformation via only basal slip and GBS. The creep rate then becomes limited by the slower of these two processes. When basal slip is faster than GBS, the creep rate is limited by the slower process, GBS, yielding a stress exponent of $n = 1.8$; when GBS is fast compared to basal slip, a stress exponent of $n = 2.4$ is obtained, and the creep data for polycrystalline samples agree with those for single crystals deformed via basal slip. With further decreasing stress, a transition to diffusion-accommodated GBS, or diffusion creep, is anticipated (Mukherjee 1971), but thus far this creep mechanism has eluded experimentalists (Goldsby and Kohlstedt 2001).

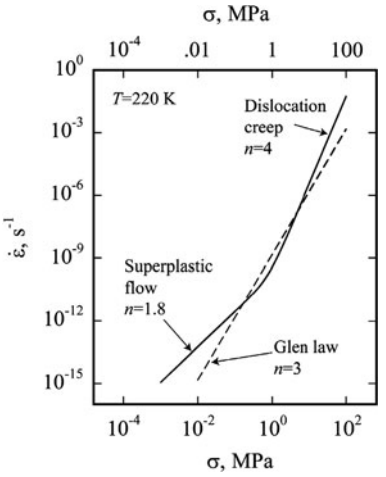

Fig. 5 Plot showing the extrapolation of the composite flow law for creep of ice I (see (5)) to 220 K and a grain size of 1 mm. *Solid line* is the composite flow law, *dashed line* is the Glen flow law with a low-temperature B parameter value (see p. 39 in Paterson 1994). The Glen law, obtained over a limited range of stresses from ~0.1 to <10 MPa, is an average of the flow behaviors in the superplastic flow and dislocation creep regimes

The rheological behavior described above is embodied in the following semi-empirical composite flow law (Goldsby and Kohlstedt 2001):

$$\dot{\varepsilon} = \dot{\varepsilon}_{\text{diff}} + \left(\frac{1}{\dot{\varepsilon}_{\text{basal}}} + \frac{1}{\dot{\varepsilon}_{\text{GBS}}} \right)^{-1} + \dot{\varepsilon}_{\text{disl}}. \tag{5}$$

The subscripts from left to right denote diffusion creep, basal slip-limited GBS creep, GBS-limited basal slip creep, and dislocation creep. Each term is a flow law of the general form of (2).

3.5 GSS Creep in Ice II

GSS creep can generally be expected on theoretical grounds to operate in any crystalline materials if stresses are sufficiently low. Ice II has recently become the second planetary ice phase to exhibit unambiguously such rheological behavior in the laboratory (Kubo et al. 2006). Synthesizing fine-grained high-pressure water ice is problematic because of the high pressures required, but Kubo et al. were able to synthesize fine-grained ice II samples by repeatedly cycling pressure across the ice I–II phase boundary. They measured a flow law for ice II that predicts that at planetary stresses <0.01 MPa, ice II will be softer than ice I for grain sizes below 1–10 mm. It is plausible therefore that GSS creep in ice II defines the rheological behavior of the potentially large volume of ice II that must exist within the large icy moons of the outer solar system.

3.6 Implications for the Glen Law

A simple extrapolation of the composite flow law in (5) to a larger grain size of 1 mm, using experimentally derived flow-law parameters for dislocation creep and GBS-limited creep, and estimated or measured parameters in the diffusion creep equation (given in Goldsby and Kohlstedt 2001), is shown in Fig. 5. The Glen law for ice is also plotted in the figure for comparison. As can be seen in Fig. 5, the Glen law essentially intersects the transition region between GBS-limited flow and dislocation creep of ice. This comparison indicates that the Glen law is not representative of one creep mechanism, but is rather a composite

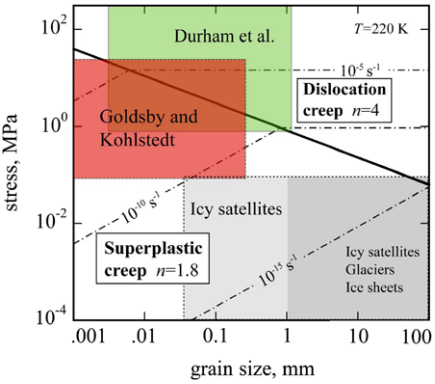

Fig. 6 Deformation map for ice I at 220 K. Conditions of experiments of Goldsby and Kohlstedt (see text for the references) are shown in *red box*; conditions of Durham et al. experiments are shown in *green* (see text for the references). The *solid line* is the boundary between the superplastic flow and dislocation creep regimes

of (i.e., contains contributions from) two creep mechanisms, dislocation creep proper, with $n = 4$, and GBS-limited creep, with $n = 1.8$, leading to an intermediate value of the stress exponent ($n = 3$). This is likely not a coincidence, but rather may be a confirmation of the 'field boundary hypothesis' of de Bresser and co-workers, described below. Hence, the Glen law significantly underestimates the strain rate in natural ice bodies and in planetary environments. This is consistent with the very common observation that ice flow in glaciers and ice sheets, for example, is faster than predicted by the Glen law, requiring rather arbitrary 'enhancement factors' to compensate (Paterson 1994).

3.7 Glaciological and Planetary Implications

A simple extrapolation of laboratory-derived flow laws for superplastic flow and dislocation creep to grain sizes encountered in terrestrial glacier and ice sheets, and to reasonable planetary grain sizes and stresses, strongly suggests that GBS limits the flow of ice over most temperatures at stresses <0.1 MPa. An example of such an extrapolation is illustrated in the deformation mechanism map in Fig. 6. The map is drawn on axes of grain size and stress, for a constant temperature of 220 K. The solid line in the figure delineates the boundary between regions of stress–grain size wherein dislocation creep and GBS-limited creep dominate the strain rate, and lines of constant strain rate are overlain in the figure. As shown on the map, at nearly all conditions of grain size and stress encountered within icy satellites and terrestrial ice bodies, the creep rate is expected to be dominated by GBS-limited flow. It is only at the base of glaciers and ice sheets, for example, where stresses are highest, that the ice nears or encounters the transition to the dislocation creep regime. Similarly, estimates of, for example, convective stresses in icy satellites indicate stresses $\ll 1$ MPa; for reasonable estimates of ice grain sizes based on terrestrial analogs, one also concludes that the flow of planetary ices is limited by GBS-limited flow. Thus, the flow law for superplastic creep has been employed in successfully modeling a host of planetary ice flow phenomena, including crater relaxation on Ganymede (Dombard and McKinnon 2000), flow of the Martian polar ice caps (Nye 2000; Nye et al. 2000), grooved terrain formation on Ganymede (Dombard and McKinnon 1996), convection in Europa's outer icy shell (Pappalardo et al. 1998; Nimmo and Manga 2002) and flow of periglacial features on Mars (Milliken et al. 2003).

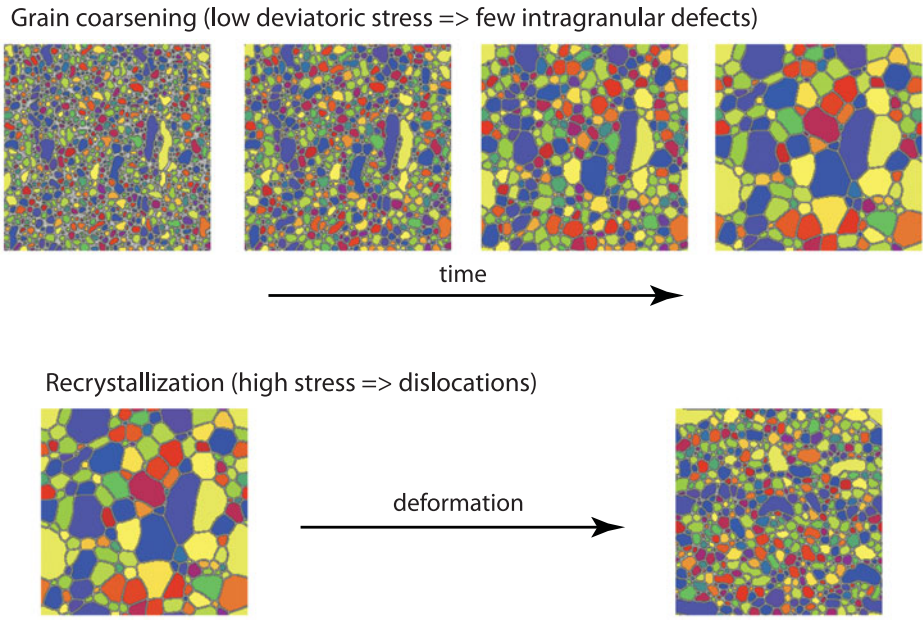

Fig. 7 Computer-generated cartoon of grain growth (*top*) and grain size reduction by recrystallization under stress (*bottom*) in a polycrystal. Grain growth requires only time and is ongoing, so when stress is applied, the two processes act simultaneously, suggesting that grain size may reach a dynamic balance (after Y. Suwa and Y. Saito, Waseda University, Tokyo, http://www.msm.cam.ac.uk/phase-trans/abstracts/grain.movies.html)

3.8 Recent Topics of Interest

3.8.1 Grain Size Distribution and the Dynamic Balance of GSS and GSI Creep

As described above, GSS creep in ice I and ice II, deformation mechanisms of the very utmost planetary relevance, have been observed and measured in the laboratory. However, it is important to recognize that grain size in solid materials is not necessarily a free variable. As depicted in Fig. 7, grains can grow (coarsen) by annealing, the process of lowering internal energy by lowering the amount of grain boundary area per unit volume. Grain size can also decrease, especially during deformation, through processes of dynamic recrystallization. Both processes can be understood from a thermodynamic perspective: in grain coarsening, internal energy is lowered by lowering the density of grain boundary area per unit volume; in dynamic recrystallization, the internal energy of large, dislocation-filled grains is lowered by replacing them with dislocation-free grains. In the latter case, self-organizational instabilities during the recrystallization process lead to an increase in grain boundary area per unit volume (i.e., smaller grains), but the net change in internal energy is still a decrease.

Operation of the GSS mechanism of diffusion creep does not promote the multiplication of line defects (dislocations) so that there is no thermodynamic driving force for reducing the density of these defects by nucleating new grains; grain growth therefore occurs readily in the diffusion creep regime. Dislocation slip in a dislocation-accommodated GBS regime may increase the density of dislocations and provide a driving force for nucleation of new grains, and thus grain growth may be at least somewhat suppressed compared to that in the diffusion creep regime. In contrast, GSI creep can be expected to generate planar and line

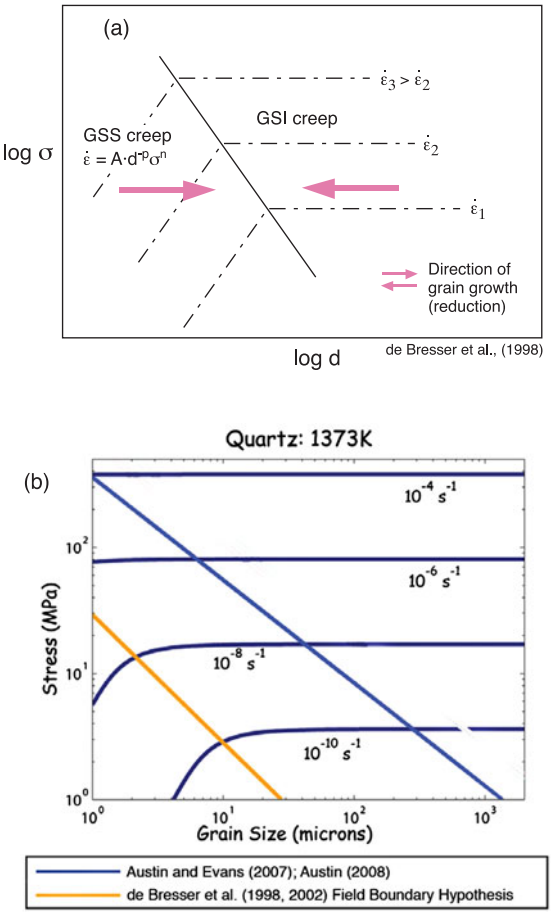

Fig. 8 Development of field boundary hypothesis for dynamic grain size distribution during deformation. (**a**) Deformation map including a portion of regions dominated by GSS and by GSI creep, illustrating that grain size reduction, active only during GSI creep, and grain growth, active at all times, act to push grain size in the direction of the boundary of the two regions, and (**b**) suggested variation of the field boundary hypothesis by Austin and coworkers for the case of polycrystalline quartz

defects in large numbers and therefore will strongly promote grain-size reduction processes, i.e., dynamic recrystallization. The driving force for grain nucleation due to grain boundary migration and bulging is particularly large in the GSI creep regime, where slip on multiple slip systems oriented for easy and hard slip can yield grains of very different internal strain energies; this strain energy mismatch drives boundary migration and recrystallization. De Bresser and colleagues (De Bresser et al. 1998, 2001; Kellermann Slotemaker and de Bresser 2006) noted that the differing effects of GSI and GSS creep on grain size act at cross purposes with respect to their respective dominance of creep rate (Fig. 8a). They hypothesized that during creep grain sizes evolve to a distribution such that GSS and GSI mechanisms contribute approximately equally to the overall creep rate, their so-called "field-boundary" hypothesis. Austin and Evans (2007) have taken this one step further to hypothesize that the dynamic distribution of grain size thus created is also influenced by the rate at which GSI creep generates intracrystalline defects, which in turn is proportional to the rate of work (i.e., power) dissipated in GSI creep. Where paleo-strain rate can be estimated in an exposed rock formation that has undergone natural deformation, measured grain size of the rock compared against that at the theoretical field boundary (Fig. 8b) becomes an effective "paleowattmeter" for the particular tectonic setting.

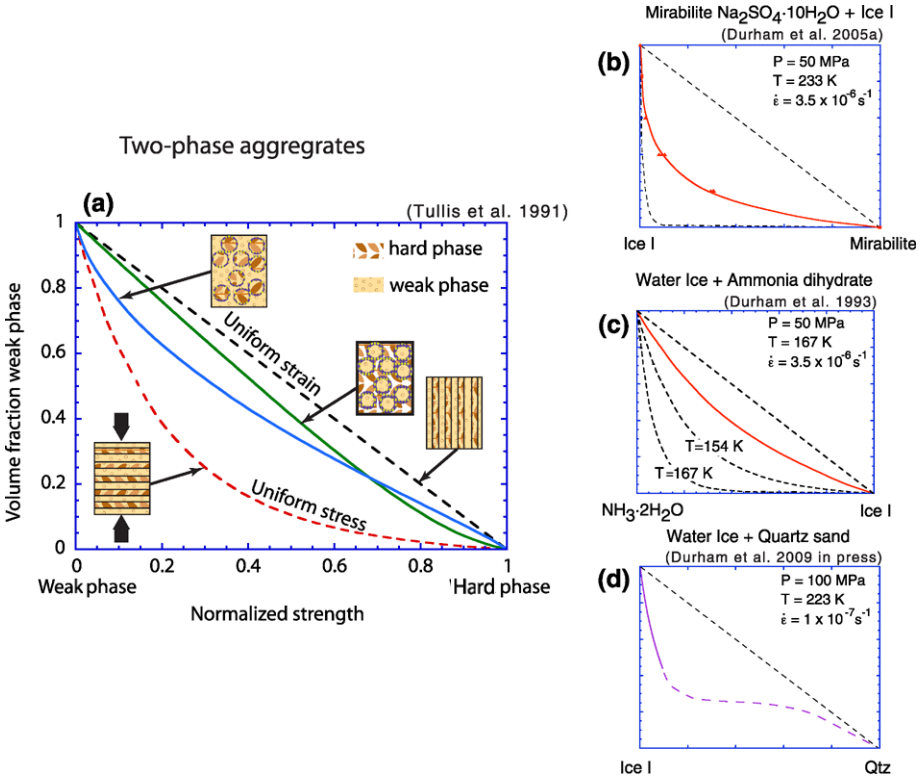

Fig. 9 Rheological behavior of two-phase mixtures. (**a**) General concepts, (**b**)–(**d**) specific icy mixtures of planetary interest. In all plots, normalized strength on the *horizontal axis* varies linearly from 0 to 1, where 0 is the strength of the harder phase and 1 is that of the softer

3.8.2 Rheological Behavior of Multiphase Systems

The rheological properties of systems of more than one phase are complex and diverse. Efforts to date to generalize relationships for the flow of multiphase system have often been inspired but have mostly been unsuccessful (Bloomfield and Covey-Crump 1993; Ji 2004; Treagus 2003; Tullis et al. 1991). Predictably, the best quantitative models occur where phases have the least contrasting rheologies. Figure 9(a), taken from Tullis et al. (1991), illustrates a range of behaviors for simple geometric arrangements of two-phase systems. The "normalized strength" on the horizontal axis of the plot runs from 0, where the strength of the aggregate has the strength of the weaker phase, to 1, where the aggregate strength is that of the harder phase. At one extreme, where the two phases are constrained to strain at the same rate, as with a geometric arrangement of vertical layers with the direction of a uniaxial stress parallel to the layers, the strength of the aggregate is linearly proportional to the volume fractions of the phases. At the other extreme, where both phases experience the same stress, as with horizontal layers lying normal to the uniaxial stress, deformation of the weaker phase will dominate the flow, and the strength of the aggregate for any given choice of volume fractions between 0 and 1 will be much weaker than for the case of uniform strain. Intermediate geometries exhibit intermediate behaviors.

Examples of specific binary systems of planetary ices are shown in Fig. 9, (b to d). In 9(a), mirabilite, a hydrated sulfate salt that is a surrogate for candidate hydrated salts on the Europan crust (Dalton et al. 2010, this issue) is far stronger than ice I, but still deformable. Quasi-uniform mixtures (i.e. not layers or columns) of mirabilite + ice I show dominance of ice I rheology for all but the mirabilite-richest (say, >0.67) mixtures (Durham et al. 2005b). In Fig. 9(c), mixtures of ammonia dihydrate (the elusive planetary ice phase) and water ice I show a composition-strength curve whose shape is very strongly temperature-dependent, reflecting the decrease in rheological contrast between the phases with temperature. Pure ammonia dihydrate is orders of magnitude less viscous than ice I near its melting point at $\sim$173 K (Fig. 3), but has the same viscosity as ice I at 143 K (Durham et al. 2003; Hogenboom et al. 1997). For mixtures of undeformable quartz sand + ice I (Fig. 9d), the strength of the weak phase dominates over much of the compositional range (Durham et al. 1992), although an inflection point is introduced into the curve because at low concentrations of ice, <0.25 (Durham et al. 2009), the aggregate remains nearly undeformable because quartz particles continue to form a rigid, load-bearing framework after a small amount of strain. Note the similar shape in one of the curves in Fig. 9(a).

In real systems of more than one phase, special textures which influence grain–grain interactions can be expected to affect rheological behavior in ways that cannot be modeled employing idealized geometries. In particular, compositional foliation (Jordan 1987) and other forms of phase segregation (Holtzman et al. 2003; Holtzman and Kohlstedt 2007) can cause unexpected rheological influences of one phase or the other, depending on the stress conditions. Finely textured, complex, intimate intergrowths, like alloy structures of metals, are seen in frozen magnesium sulfate–water mixtures (McCarthy et al. 2003, 2004, 2007). Such intergrowths of rheologically disparate minerals as ice and epsomite are expected to yield deformational behavior unlike either of the end-members; however, this behavior has not been fully investigated. One may expect that crustal domains of Europa (and other bodies) that contain large concentrations of such intergrowths (such as frozen cryovolcanic brine flows) would be rheologically decoupled from the ice-dominated crust as a whole. Hence, salt-rich domains may have distinct tectonic structures associated with them, thus helping to explain the distinctive geological nature of the salt-rich zones observed on Europa. The tidal response of ice shells overlying oceans in bodies such as Europa, including heat generation from tidal dissipation, might also be affected by any widespread occurrence of such materials in the icy shell. Such phenomenology has not been investigated to date.

4 Thermal Properties of Some Minerals in Icy Satellites. The Case of Hydrated Salts

4.1 Introduction

Thermal properties of a planetary body's materials determine its activity, geological evolution, and in the case of the icy satellites, even the existence of potential habitable environments. Planetary thermal energy may be produced by accretion and global differentiation (release of gravitational potential energy), impacts (release of kinetic energy), decay of radioactive elements, dissipation of tidal stress, dissipation of frictional energy during faulting and release of stored lattice strains caused by other tectonic motions, electrical resistance, and exogenic chemical reactions during chemical equilibration. Some of these energy sources are linked and flow from one energy pool to another (for instance, radioactive heating can lead to buoyant forces, and those may cause faulting and shear heating). The end result is heating of planetary interiors; this energy then can be dissipated through the body

by advective processes such as magmatism and solid-state convection as well as by thermal conduction.

Heat transfer and establishment of the thermal state and geophysical dynamics of a body are governed by melting points, latent heats of phase transitions, thermal conductivity, specific heat and thermal expansivity, and temperature-dependent rheological behavior governing solid-state deformation, tectonics, and advective heat transfer, as well as all relevant length scales (e.g., satellite radius). Partial melting of the original accreted materials (or of reequilibrated/recrystallized primitive materials), and then advective mass transfer (e.g., magmatism) driven by differences in density of the products of partial melting, are primarily responsible for the large-scale structure of planetary interiors. The global thermal state and tectonics of a body are in turn affected by the material layering and will consequently evolve with the configuration of the materials. This endogenous activity may be detected at the surface since it is manifested in recognizable geological features, such as flows, dispersed deposits around a local source, domes, and tectonic patterns of faults. Formation of global aqueous oceans or disconnected liquid reservoirs in icy satellites, which may be maintained for long periods of interest both geologically and biochemically, is either allowed or restricted by the thermal state history of the object. Accordingly, habitability of the aqueous environments in the outer solar system is controlled in some way by the thermal conductivity and other thermodynamic properties of major compounds that accompany the required liquid water. Not only are non-water substances important as sources of biochemicals, but also for control of heat transfer and stability of liquid water habitat.

Classically, studies of icy satellites have considered only pure compositions (usually water ice, sometimes different phases) in calculations, neglecting the influence of other constituents on the thermal state. The predominance of exotic cryogenic solid materials in the icy satellites, compared with the familiar silicates of terrestrial planets, represents a challenge in modeling endogenous planetary processes. As new data about surface and interior chemistry and mineralogy of icy satellites and geophysical constraints on their interior structures are obtained from space missions, as geological observations are made about key processes, and theoretical models of key processes are produced, laboratory experimentalists generate new data relevant to these materials and processes. Through this interactive science community-based effort of observation, interpretation, and theoretical application, we gain an improved understanding of the outer solar system icy bodies and derive insights relevant to planetary science in general. The significance of major non-ice constituents in icy satellites is therefore largely due to their contrasting physical-chemical properties, especially different thermal conductivities, relative to water ice.

Ices in the outer solar system are diverse, and their distributions depend on the location, especially distance from the Sun. Water ice is the most abundant and widespread volatile and may appear in different phases depending on the stability conditions of pressure and temperature and abundances of other constituents with which it may either react chemically or form hydrates. Molecular ices, salt hydrates and clathrate hydrates are also relevant to the solid compositions of the icy satellites. Hydrated salts are usually formed in terrestrial planets by evaporation of water from concentrated solutions, and by crystallization at low temperatures in icy satellites. Signatures of hydrates associated with some geological features have been detected by near-infrared spectroscopy on the surface of Europa and Ganymede. They have been interpreted as hydrated salts or hydrates of sulfuric acid (McCord et al. 1998; Carlson et al. 1999; Dalton et al. 2005). As we will see below, they may play an important role in the activity of the Jovian satellites (Kargel et al. 2000; Prieto-Ballesteros and Kargel 2005).

Aqueous cryomagmatism is interesting not just for geology and geophysics, but also for astrobiology. Chemical systems with water, which are present in the icy satellites, have lower

melting points than pure water (see Fortes and Choukroun 2010, this issue). This means that aqueous liquids may occur in the interior, even if the temperature is extremely low. Ammonia and methanol are very effective melting point depressants; for example, the peritectic of the ammonia–water system is at 176.1 K, and a eutectic occurs at 175.4 K (Hogenboom et al. 1997). Methanol–ammonia–water and some other frozen aqueous systems melt at even lower temperatures (Kargel 1992). Because ammonia hydrate is a predicted condensable volatile in the Solar Nebula, expected to be the second most widespread volatile after water ice (Lewis 1972), and because of its low melting temperature and expected high abundance in some nebula condensation scenarios, ammonia–water has commonly been assumed to be a system that leads to formation of the aqueous reservoir in the interior of icy satellites, such as Enceladus (Croft et al. 1988; Kargel et al. 1991, 1992; Kargel and Pozio 1996; Roberts and Nimmo 2008) or Titan (Mitri et al. 2008; Choukroun et al. 2009).

Other expected freezing-point depressants include salts, which may be present in the satellites of Jupiter, Europa or Ganymede (Kargel 1991; Kargel et al. 2000; Prieto-Ballesteros and Kargel 2005). The expected presence of salts in icy satellites is due to a set of hydrolysis reactions similar to those caused by aqueous weathering of the Earth's surface; however, differences in modeled compositions, conditions, and reaction pathways in icy satellites lead to different modeled relative and absolute abundances of various salts, and in some cases some different types of salts, in icy satellites compared to Earth and other mainly silicate bodies (Kargel et al. 2000; Zolotov and Kargel 2008). Chlorides have lower eutectic points than sulfates in water systems, but they have not been detected yet in any icy satellite, with the exception of small amounts of sodium chloride discerned in particulate ejecta from Enceladus' plumes (Schneider et al. 2009; Postberg et al. 2009). Sodium chloride also is believed to be present on Io, a non-icy outer planet satellite (Lellouch et al. 2003; Carlson et al. 2006); in that case, volcanic exhalative processes appear to be responsible for the salt. Pure or mixed anhydrous molecular ices (CH_4, CO_2, CO, N_2) have extremely low melting points. However, methane and ethane may exist in liquid phase at the surface of Titan, stabilized by the pressure of the atmosphere. They form ponds or even seas (Lunine et al. 1983; Lorenz et al. 2003; Stofan et al. 2007), which are part of the dynamical exogenous cycle of this satellite.

4.2 Thermal Behavior of Hydrates at Low Temperatures

Heat capacity and thermal conductivity are properties of chemical compounds that may be measured experimentally, but it is common to find some discrepancies among authors because of the use of differing methodologies and configurations of sample materials.

Vibrations on the crystal lattice, crystal disorder, and magnetic and electric properties determine the heat capacity and thermal conductivity of solids. Each parameter affects to different degrees each type of mineral or condensate. For instance, electric and magnetic contributions are important in metal-bearing minerals, while crystallinity strongly affects the silicate frameworks or lattices of hydrated salts. To explain the theory of conduction of covalent and ionic minerals is beyond the scope of this chapter, but it is important to note that heat transport is due to a phonon movement, which is analogous to photon movement in radiation energy. Some scattering is produced when phonons interact, due to the non-harmonic nature of thermal vibrations. The mean free path between collisions will determine the value of thermal conductivity, and this value will generally be higher when the path is longer. Crystalline materials usually have higher thermal conductivity at low and medium temperatures (which are the temperatures of interest for studies of icy satellites) than at high. This is because at low temperatures there are longer mean free paths at lower amplitudes and

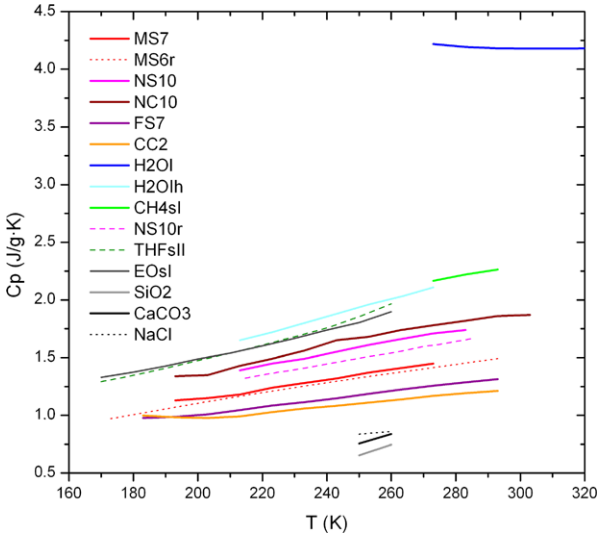

Fig. 10 Heat capacity (C_p) of some compounds of planetological interest as function of temperature. Liquid water, H_2O-I, SiO_2, $CaCO_3$, and NaCl data are from Lide (2008); THF-sII (tetrahydrofuran structure II clathrate) and EO-sI (ethylene oxide structure I) are from White and MacLean (1985), CH_4-sI is from Waite et al. (2007); NS10-r is from Brodale and Giauque (1958); MS6-r is from Cox et al. (1955); MS7 ($MgSO_4 \cdot 7H_2O$, epsomite), NS10 ($NaSO_4 \cdot 10H_2O$, mirabilite), NC10 ($Na_2CO_3 \cdot 10H_2O$, natron) are from Prieto-Ballesteros and Kargel (2005); FS7 ($FeSO_4 \cdot 7H_2O$, melanterite) and CC2 ($CaCO_3 \cdot H_2O$, gypsum) are new data. Data for the last two hydrated salts have been obtained following the same methodology than those published in Prieto-Ballesteros and Kargel (2005), by MDSC

more harmonicity of the thermal vibrations. Phonon scattering is also less when cations are close to the atomic weight of anions. Another observed fact is that it is common that crystals with complex structures have lower thermal conductivities than more simple structures.

4.2.1 Heat Capacity (C_p)

Heat capacity is defined as the amount of heat required to increase by one degree the temperature of one mole of a substance; alternatively, it may be defined on a per-unit-mass basis. Here we use units of joules/gram-Kelvin. Heat capacity depends on the mass, chemical composition, the thermodynamical state and the process that is involved in the heat transfer. Heat capacity in aqueous systems depends on the composition and concentration of solutes.

Heat capacity at atmospheric pressure as a function of temperature for several species of planetological interest, including hydrated salts, water ice I and clathrate hydrates may be seen in Fig. 10. Laboratory experiments show that hydrated salts have specific heat values 15–65% lower than that of water ice, with the lowest values found for anhydrous salts (Fig. 10). Comparison of data obtained at room temperature for several salt hydration states demonstrates that the specific heat increases as the number of water molecules increases (Prieto-Ballesteros and Kargel 2005). Clathrate hydrates also have values of specific heat similar to that of water ice I. It has been observed that specific heat values for clathrates are slightly dependent on guest molecule and occupancy of the cages (Andersson and Ross 1983; Handa and Tse 1996; Tombari et al. 2006).

Considering that internal aqueous oceans may exist in some icy satellites, the specific heat of aqueous solutions has also been explored. There are many references in the literature

about the apparent molar heat capacity of some solutions. Data are mostly for halides and are usually obtained from room to higher temperature (Randall and Rossini 1929; Randall and Taylor 1941; Simard and Fortier 1981; Picker et al. 1974). In general, salty aqueous solutions with low and moderate salt concentrations have specific heat values that are similar to or slightly less than that of pure liquid water. Higher concentrations of solutes increase the specific heat. The effect of sulfuric acid in solutions with other salts is remarkable. Bhattacharyya and Bhattacharyya (1979) showed that higher concentrations of the acid (25%) in an aqueous system also containing ferrous sulfate decreased the heat capacity of the solution.

4.2.2 Thermal Conductivity

Thermal conductivity measures the ability of a material to conduct heat. In the same manner as specific heat, thermal conductivity depends on many properties of the material, particularly its chemical composition and structure. For instance, pure crystalline substances may exhibit very different thermal conductivities along different crystal axes.

The thermal conductivity of a rock is determined by the conductivities of its mineral constituents, by the pore structure, and by the conductivities of the fluids that saturate the pores. A similar situation exists for assemblages of low-temperature solid phases in icy satellites. Micro- and macro-structure of the assemblage is critical in determining the conductivity, so porosity, lattice anisotropy, or schistosity of samples must be controlled in laboratory experiments and taken into account when modeling.

In considering the thermal conductivity materials are in general grouped as being either conducting or insulating. Values of thermal conductivity in the range 10 to 400 W/m·K are typical for conductors, while insulators are below 2 W/m·K, more or less the value of water ice at around 273 K. Most terrestrial rocks and minerals have conductivities between 1 and 10 W/m·K. For our purposes, we consider materials that are more conductive than water ice to be conducting and materials less conductive than water ice to be insulating. An extensive review of thermal conductivity of ices in the solar system is given in Ross and Kargel (1998). These authors compiled data for the most relevant ices of the solar system (water ice, CO_2, CH_4, N_2, amorphous ice, clathrate hydrate), showing the different conductivities of the polymorphs of ice with pressure, as well as the inverse dependence of conductivity on temperature of amorphous solids and crystalline clathrate hydrates. Thermal conductivity of water ice I at atmospheric pressure is very well known (Slack 1980), but there are few data for other ices. Only limited data exist for thermal conductivity at high pressure. The best-studied ice at high pressure is water ice. High pressure polymorphs of ices II, III, IV, V, VI, and IX have lower thermal conductivities than I, while VII and VIII have higher values. All the water phases have the dependence with temperature typical of crystalline solids (Ross et al. 1978; Dharma-Wardana et al. 1983).

Because of possible economic importance of some gas clathrates, their properties are being analyzed in detail. All clathrates studied to date have similar thermal conductivities (about 0.5–0.7 W/m·K) for temperatures from 50 K to near the melting point (Ross et al. 1981; Andersson and Ross 1983; White and MacLean 1985; Handa and Cook 1987; Waite et al. 2007; Rosenbaum et al. 2007). It is worth nothing that the thermal conductivity of clathrate hydrates exhibits a slightly inverse dependence with temperature. This behavior is typical of glassy solids, but it has been alternatively explained by a different hypothesis: by the low frequency rattling of the guest molecule in the cage, resulting in strong scattering of the thermal phonons (Tse and White 1988; Ross and Kargel 1998), and by tunneling states arising from proton disorder (Phillips 1972; Ahmad and Phillips 1987). In addition to this, the thermal conductivity of clathrate hydrates is apparently independent of pressure.

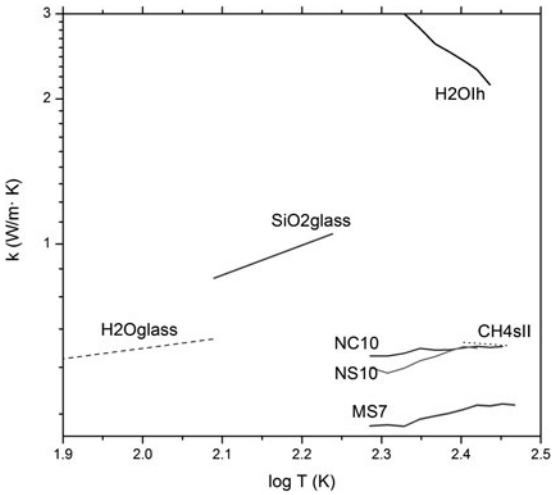

Fig. 11 Dependence of thermal conductivity (k) on temperature for some minerals and condensates of planetological interest. Material abbreviations same as Fig. 10. Data for H_2O-I are from Slack (1980), glassy-H_2O from Andersson and Suga (1994), glassy SiO_2, crystalline SiO_2 and NaCl are from Lide (2008), THF-sI is from Tse and White (1988), CH_4-sI (structure I methane clathrate) is from Waite et al. (2007); MS7, NS10 and NC10 are from Prieto-Ballesteros and Kargel (2005)

It is noticeable that measurements of thermal conductivity of some hydrated salts show very similar behavior (Fig. 11). Thermal conductivity data obtained at atmospheric pressure from some magnesium- and sodium-hydrated sulfates and carbonates have values a third or fourth lower than that of water ice (Prieto-Ballesteros and Kargel 2005). In addition, at low to medium temperatures the thermal conductivities of hydrated sulfates and carbonates also decrease when temperature increases, in the same manner as for clathrate hydrates. The molecular structures of clathrate hydrates and hydrated sulfates may be described in a simple way as being formed by guest molecules surrounded by a cortex of water molecules. If the similar thermal behavior is due to the water molecules' configuration, then arguments previously mentioned for clathrate hydrates may be applied to hydrated salts. In sharp contrast with the hydrates, anhydrous salts, notably halite and anhydrite, are more conductive than water ice.

Some authors have explored the thermal properties of porous materials (H_2O, CO_2, mineral powders and some of their mixtures), which are typical of comets (Komle et al. 1996; Seiferlin et al. 1995, 1996; Steiner and Kömle 1991). Measurements of these mixtures were made at vacuum conditions and, as expected, gave very low values. As an example, porous fine-grained ice measured from 80 to 240 K have values of thermal conductivity in the range 0.005–0.15 W/m·K, while mixtures of ice and silicate minerals have values from 0.1 to 4 W/m·K (Seiferlin et al. 1996; Prialnik et al. 2004).

4.2.3 Planetological Thermal Effects of the Paradoxical Hydrates

Traditionally, ice I has been used to model processes occurring in the icy satellites. However, the other compounds that have been detected by spacecraft sensors must also be taken into account. In some cases, these materials are associated with geological features such as fractures or cryomagmatic structures. This is the case for the hydrated salts on the surface of Europa.

The analysis of the thermal properties of these hydrates indicates that they may favor geological activity more than pure water ice; either the hydrates are the product of this activity, or they spur this activity, or both. Assuming that there exist significant amounts of hydrated salts on Europa, the low thermal conductivity of the salt-rich zones may result in better heat retention than if the mineralogy was dominated by water ice. Steeper thermal

gradients would result for a given input of heat if large amounts of hydrates are present in the interior of Europa (Prieto-Ballesteros and Kargel 2005). Some effects of this gradient are a thinner floating crust and an ocean closer to the surface, a shallower depth to partial melting, or a shallower onset of convective conditions.

On the other hand, aqueous solutions, including pure liquid water, may store heat due to their high specific heat and latent heats, while hydrates may act as thermal insulators. If hydrated salts are present in an icy body, the combination of heat capacity and thermal conductivity would result in the liquid reservoirs sustained for long times. Insulation tends to prevent heat loss and to stabilize subsurface liquids (brine plutons or an ocean), which may be more potent than effects due to solute-induced freezing-point depression, but both insulation and freezing point depression work together to make melting more likely than in the absence of salts. The high strength and low ductility of salt hydrates compared to ice also helps to inhibit solid-state convection, and thereby also increase chances of melting compared with situations where the salts are absent. The inverse dependence of conductivity on temperature for salt hydrates and clathrate hydrates means that they are better insulators at lower temperatures (close to the surface of the satellite), but become more ice-like in their conductivity as the water melting point is approached. This temperature dependence is opposite that of crystalline water ice and most other crystalline materials.

Considering the presence of a briny ocean, the impact of salt hydrates on thermal gradient is probably even greater in the suboceanic region, where a thick subcrust of pure salt hydrates may occur (Kargel et al. 2000; Prieto-Ballesteros and Kargel 2005). (Note, however, the possibility of other scenarios, where the salts would not be so abundant; see Zolotov and Kargel 2008.) Salts would form from aqueous solution and precipitate to the ocean bottom due to their higher density. If hydrates are not mixed with other conducting minerals, the thermal gradient may be even steeper here than in the floating salty ice crust. However, this effect may be self-limiting, because high temperatures would cause dehydration of salts and an increase in thermal conductivity to values more like those of silicate rock and ordinary ice I. This effect has been explored also for Mars (Kargel et al. 2007).

If salts are distributed inhomogeneously in Europa's crust, large lateral gradients in subsurface thermal structure and geologic activity would be likely. The next mission to the Jupiter system and Europa should try to confirm the association of local thermal anomalies with the material type and geological structure. Intruded brine dikes and plutons and extruded brine lava flows would cool much more slowly than equivalent water bodies. This may have significance for the future thermal prospecting of geologic activity on Europa and other icy bodies, since thermal emissions due to shallow brine bodies may be extended over greater periods of time before the bodies freeze solid and cool to ambient conditions. The main objective of a future mission to Europa and the rest of the Jovian system may be to search for potentially habitable environments, characterizing any aqueous reservoir in the satellites in a first step. It will be essential to know the thermal properties of the materials in order to understand the thermal state of the satellite. Although there are already some existing thermal properties data for planetary ices, most were obtained at terrestrial conditions. Hence, much work on thermal properties under specific planetary conditions (from the interior to the surface) still needs to be done in order to prepare for future exploration of the icy bodies of the solar system.

References

N. Ahmad, W.A. Phillips, Thermal-conductivity of ice and ice clathrate. Solid State Commun. **63**(2), 167–171 (1987)

R.B. Alley, Flow-law hypotheses for ice-sheet modeling. J. Glaciol. **38**, 245–256 (1992)
P. Andersson, R.G. Ross, Effect of guest molecule size on thermal conductivity and heat capacity of clathrate hydrates. J. Phys. C. Solid State Phys. **16**, 1423–1432 (1983)
O. Andersson, H. Suga, Thermal conductivity of low density amorphous ice. Solid State Comm. **91**(12), 985–988 (1994)
M.F. Ashby, R.A. Verrall, Diffusion-accommodated flow and superplasticity. Acta Metall. **21**, 149–163 (1973)
N.J. Austin, B. Evans, Paleowattmeters: A scaling relation for dynamically recrystallized grain size. Geology **35**(4), 343–346 (2007)
A. Ball, M.M. Hutchinson, Superplasticity in the aluminum-zinc eutectoid. Metal Sci. J. **3**, 1–7 (1969)
S. Bhattacharyya, S.N. Bhattacharyya, Heat-capacity and enthalpy of the ternary-system ferrous sulfate heptahydrate, sulfuric-acid, and water. J. Chem. Eng. Data **24**(2), 93–96 (1979)
J.P. Bloomfield, S.J. Covey-Crump, Correlating mechanical data with microstructural observations in deformation experiments on synthetic 2-phase aggregates. J. Struct. Geol. **15**(8), 1007–1019 (1993)
G.E. Brodale, W.F. Giauque, Heat of hydration of sodium sulfate. Low-temperature heat capacity and entropy of sodium sulfate decahydrate. J. Am. Chem. Soc. **80**, 2042–2024 (1958)
W.F. Budd, T.H. Jacka, A review of ice rheology for ice sheet modelling. Cold Reg. Sci. Technol. **16**, 107–144 (1989)
B. Burton, *Diffusional Creep of Polycrystalline Materials* (Trans. Tech. Publications, Germany, 1977), 119 pp.
R.W. Carlson, R.E. Johnson, M.S. Anderson, Sulfuric acid on Europa and the radiolytic sulfur cycle. Science **286**, 97–99 (1999)
R.W. Carlson, J.S. Kargel, S. Doute, L.A. Soderblom, J.B. Dalton, Io's surface composition, in *Io after Galileo*, ed. by R.M.C. Lopes, J.R. Spencer (Springer, Berlin, 2006)
M. Choukroun, O. Grasset, G. Tobie, C. Sotin, Stability of methane clathrate hydrates under pressure: Influence on Titan's cryovolcanism and atmospheric methane replenishment. Icarus (2009). doi:10.1016/j.icarus.2009.08.011
R.L. Coble, A model for boundary diffusion controlled creep in polycrystalline materials. J. Appl. Phys. **34**, 1679–1682 (1963)
W.P. Cox, E.W. Hornung, W.F. Giauque, The spontaneous transformation from macrocrystalline to microcrystalline phases at low temperatures. The heat capacity of $MgSO_4 \cdot 6H_2O$. J. Am. Chem. Soc. **77**(15), 3935–3938 (1955)
S.K. Croft, J.I. Lunine, J. Kargel, Equation of state- of ammonia-water liquid—Derivation and planetological applications. Icarus **73**, 279–293 (1988)
J.B. Dalton et al., Space Sci. Rev. (2010, this issue)
J.B. Dalton, O. Prieto-Ballesteros, J.S. Kargel et al., Spectral comparison of heavily hydrated salts with disrupted terrains on Europa. Icarus **177**, 472–490 (2005)
J.H.P. De Bresser, C.J. Peach, J.P.J. Reijs, C.J. Spiers, On dynamic recrystallization during solid state flow: Effects of stress and temperature. Geophys. Res. Lett. **25**, 3457–3460 (1998)
J.H.P. De Bresser, J.H. Ter Heege, C.J. Spiers, Grain size reduction by dynamic recrystallization: Can it result in major rheological weakening? Int. J. Earth Sci. **90**(1), 28–45 (2001)
M.W.C. Dharma-Wardana, F. Perrot, G.C. Aers, Effective proton-proton potential in hydrogen plasmas. Phys. Rev. A **28**, 344–349 (1983)
A.J. Dombard, W.B. McKinnon, Formation of grooved terrain on Ganymede: Extensional instability mediated by cold, diffusional creep. Lunar Planet. Sci. Conf. **27**, 317–318 (1996)
A.J. Dombard, W.B. McKinnon, Long-term retention of impact crater topography on Ganymede. Geophys. Res. Lett. **27**, 3663–3666 (2000)
W.B. Durham, H.C. Heard, S.H. Kirby, Experimental deformation of polycrystalline H2O ice at high pressure and low temperature: Preliminary results. J. Geophys. Res. **88**, B377–B392 (1983)
W.B. Durham, S.H. Kirby, L.A. Stern, Effects of dispersed particulates on the rheology of water ice at planetary conditions. J. Geophys. Res. **97**, 20883–20897 (1992)
W.B. Durham, S.H. Kirby, L.A. Stern, Flow of ices in the ammonia-water system. J. Geophys. Res. **98**, 17667–17682 (1993)
W.B. Durham, S.H. Kirby, L.A. Stern, Creep of water ices at planetary conditions: a compilation. J. Geophys. Res. (Planets) **102**, 16293–16302 (1997)
W.B. Durham, L.A. Stern, S.H. Kirby, Steady-state flow of solid CO2. Geophys. Res. Lett. **26**, 3493–3496 (1999)
W.B. Durham, S.H. Kirby, L.A. Stern, Rheology of ice I at low stress and elevated confining pressure. J. Geophys. Res. **106**, 11,031–11,042 (2001)
W.B. Durham, S.H. Kirby, L.A. Stern, W. Zhang, The strength and rheology of methane clathrate hydrate. J. Geophys. Res. **108**(B4), 2182 (2003). doi:2110.1029/2002JB001872

W.B. Durham, L.A. Stern, T. Kubo, S.H. Kirby, Flow strength of highly hydrated Mg- and Na-sulfate hydrate salts, pure and in mixtures with water ice, with application to Europa. J. Geophys. Res. (Planets) **110**(E12), E12010 (2005a). doi:12010.11029/12005JE002475
W.B. Durham, L.A. Stern, S.H. Kirby, S. Circone, Rheological comparisons and structural imaging of sI and sII endmember gas hydrates and hydrate/sediment aggregates, in *Proceedings of the 5th International Conference on Gas Hydrates* (paper #2030), Trondheim, Norway (2005b), pp. 607–614
W.B. Durham, A.V. Pathare, L.A. Stern, H.J. Lenferink, Mobility of icy sand packs, with application to Martian permafrost. Geophys. Res. Lett. (2009). doi:10.1029/2009GL040392
P. Duval, M.F. Ashby, I. Anderman, Rate-controlling processes in the creep of polycrystalline ice. J. Phys. Chem. **87**(21), 4066–4074 (1983)
A.D. Fortes, M. Choukroun, Space Sci. Rev. (2010, this issue)
H.J. Frost, M.F. Ashby, *Deformation Mechanism Maps* (Pergamon, New York, 1982) 167 pp.
R.C. Gifkins, Grain boundary sliding and its accommodation during creep and superplasticity. Metall. Trans. **7A**, 1225–1232 (1976)
J.W. Glen, Experiments on the deformation of ice. J. Glaciol. **2**, 111–114 (1952)
J.W. Glen, The creep of polycrystalline ice. Proc. R. Soc. Lon., Ser. A **228**, 519–538 (1955)
D.L. Goldsby, Superplastic flow of ice relevant to glacier and ice sheet mechanics, in *Glaciology and Earth's Changing Environment*, ed. by P. Knight (Blackwell, Oxford, 2006), p. 527
D.L. Goldsby, D.L. Kohlstedt, Diffusion creep in ice, in *Proceedings of the 35th U.S. Rock Mechanics Symposium*, ed. by J.K. Daemen, R.A. Schultz (Balkema, United States 1995), pp. 199–206
D.L. Goldsby, D.L. Kohlstedt, Grain boundary sliding in fine-grained Ice I. Scr. Mater. **37**, 1399–1406 (1997a)
D.L. Goldsby, D.L. Kohlstedt, Flow of ice I by dislocation, grain boundary sliding, and diffusion processes, in *Proceedings of the 28th Annual Lunar and Planetary Science Conference* (Lunar and Planetary Institute, Houston, 1997b), pp. 429–430
D.L. Goldsby, D.L. Kohlstedt, Superplastic deformation of ice: Experimental observations. J. Geophys. Res. **106**, 11,017–11,030 (2001)
D.L. Goldsby, D.L. Kohlstedt, W.B. Durham, in *Abstracts of the 24th Lunar and Planetary Science Conference*, Houston, TX, 15–19 March 1993 (1993), p. 543
Y.P. Handa, J.G. Cook, Thermal conductivity of xenon hydrate. J. Phys. Chem. **91**(25), 6327–6328 (1987)
Y.P. Handa, J.S. Tse, Thermodynamic properties of empty lattices of structure I and structure II clathrate hydrates. J. Phys. Chem. **90**, 5917–5921 (1996)
C. Herring, Diffusional viscosity of a polycrystalline solid. J. Appl. Phys. **21**, 437–444 (1950)
D.L. Hogenboom, J.S. Kargel, G.J. Consolmagno, T.C. Holden, L. Lee, M. Buyyounouski, The ammonia-water system and the chemical differentiation of icy satellites. Icarus **128**, 171–180 (1997)
B.K. Holtzman et al., Melt segregation and strain partitioning: Implications for seismic anisotropy and mantle flow. Science **301**(5637), 1227–1230 (2003)
B.K. Holtzman, D.L. Kohlstedt, Stress-driven melt segregation and strain partitioning in partially molten rocks: Effects of stress and strain. J. Petrol. **48**(12), 2379–2406 (2007)
S.C. Ji, A generalized mixture rule for estimating the viscosity of solid-liquid suspensions and mechanical properties of polyphase rocks and composite materials. J. Geophys. Res. (Solid Earth) **109**(B10), B10207 (2004)
P.G. Jordan, The deformational behavior of bimineralic limestone halite aggregates. Tectonophysics **135**(1–3), 185–197 (1987)
O.A. Kaibyshev, *Superplasticity of Alloys, Intermetallides, and Ceramics* (Springer, New York, 1992), 317 pp.
J.S. Kargel, Brine volcanism and the interior structures of asteroids and icy satellites. Icarus **94**, 368–390 (1991)
J.S. Kargel, S.K. Croft, J.I. Lunine, J.S. Lewis, Rheological properties of ammonia-water liquids and crystal–liquid slurries—Planetological applications. Icarus **89**, 93–112 (1991)
J.S. Kargel, Ammonia-water volcanism on icy satellites: phase relations at 1 atmosphere. Icarus **100**, 556–574 (1992)
J.S. Kargel, S. Pozio, The volcanic and tectonic history of Enceladus. Icarus **119**, 385–404 (1996)
J.S. Kargel, J.Z. Kaye, J.W. Head, G.M. Marion, R. Sassen, J.K. Crowley, O. Prieto-Ballesteros, S.A. Grant, D.L. Hogenboom, Europa's crust and ocean: Origin, composition, and the prospects for life. Icarus **148**, 226–265 (2000)
J.S. Kargel, R. Furfaro, O. Prieto-Ballesteros, J.A.P. Rodriguez, D.R. Montgomery, A.R. Gillespie, G.M. Marion, S.E. Wood, Martian hydrogeology sustained by thermally insulating gas and salt hydrates. Geology **35**(11), 975–978 (2007) (2007)
A. Kellermann Slotemaker, J.H.P. de Bresser, On the role of grain topology in dynamic grain growth - 2D microstructural modeling. Tectonophysics **427**(1–4), 73–93 (2006)

N.I. Komle, G. Kargl, K. Thiel, K. Seiferlin, Thermal properties of cometary ices and sublimation residua including organics. Planet. Space Sci. **44**(7), 675–689 (1996)
T. Kubo, W.B. Durham, L.A. Stern, S.H. Kirby, Grain size-sensitive creep in ice II. Science **311**(5765), 1267–1269 (2006)
T.G. Langdon, Grain boundary sliding as a deformation mechanism during creep. Phil. Mag. **22**, 689–700 (1970)
E. Lellouch, G. Paubert, J.I. Moses, N.M. Schneider, D.F. Strobel, Volcanically emitted sodium chloride as a source for Io's neutral clouds and plasma torus. Nature **421**, 45–47 (2003)
J.S. Lewis, Low-temperature condensation from solar nebula. Icarus **16**(2), 241–252 (1972)
D.R. Lide (Editor in chief). *Crc Handbook of Chemistry and Physics 2008–2009*. Editorial: Taylor & Francis 89th edition (2008)
R.D. Lorenz, E. Kraal, E. Asphaug, R. Thomson, The seas of Titan. Eos **84**, 125–132 (2003)
J.I. Lunine, D.J. Stevenson, Y.L. Yung, Ethane Ocean on Titan. Science **222**(4629), 1229–1230 (1983)
C.M. McCarthy, S.H. Kirby, W.B. Durham, L.A. Stern, Melt-grown grain textures of eutectic mixtures of water ice with magnesium- and sodium-sulfate hydrates and sulfuric-acid hydrate using cryogenic SEM (CSEM). Eos Trans. AGU **84**(46), Fall Meet. Suppl., Abstract T42A-0275 (2003)
C.M. McCarthy, S.H. Kirby, W.B. Durham, L.A. Stern, Microstructure and physical properties of sulfate hydrate/ice eutectic aggregates in the binary system sodium-sulfate/water at planetary conditions. Eos Trans. AGU **85**(47), Fall Meet. Suppl., Abstract P31A-0955 (2004)
C. McCarthy, R.F. Cooper, S.H. Kirby, K.D. Rieck, L.A. Stern, Solidification and microstructures of binary ice-I/hydrate eutectic aggregates. Am. Mineral. **92**(10), 1550–1560 (2007)
T.C. McCord et al., Salts an Europa's surface detected by Galileo's Near Infrared Mapping Spectrometer. Science **280**, 1242–1245 (1998)
R.E. Milliken, J.F. Mustard, D.L. Goldsby, Viscous flow features on the surface of Mars: Observations from high-resolution Mars Orbiter Camera (MOC) images. J. Geophys. Res. **108**, 5057 (2003) 10.1029/2002JE002005
G. Mitri et al., Resurfacing of Titan by ammonia-water cryomagma. Icarus **196**(1), 216–224 (2008)
A.K. Mukherjee, The rate-controlling mechanism in superplasticity. Mater. Sci. Eng. **8**, 83–89 (1971)
F.R.N. Nabarro, Deformation of crystals by the motion of single ions, in *Report of a Conference on Strength of Solids (Bristol)* (The Physical Society, London, 1948), pp. 75–90
F. Nimmo, M. Manga, Causes, characteristics and consequences of convective diapirism on Europa, Geophys. Res. Lett. **2**9(23) (2002)
J.F. Nye, A flow model for the polar ice caps of Mars. J. Glaciol. **46**, 438–444 (2000)
J.F. Nye, W.B. Durham, P.M. Schenk, J.M. Moore, The instability of a south polar cap on Mars composed of carbon dioxide. Icarus **144**(2), 449–455 (2000)
R.T. Pappalardo, J.W. Head, R. Greeley, R.J. Sullivan, C. Pilcher, G. Schubert, W.B. Moore, M.H. Carr, J.M. Moore, M.J.S. Belton, D.L. Goldsby, Geological evidence for solid state convection in Europa's ice shell. Nature **391**, 365–368 (1998)
M.S. Paterson, The ductility of rocks, in *Physics of Strength and Plasticity*, ed. by A.S. Argon (MIT, Cambridge, 1969), pp. 377–392
W.S.B. Paterson, *The Physics of Glaciers*, 3rd edn. (Pergamon, Oxford, 1994), 250 pp.
V.F. Petrenko, R.W. Whitworth, *Physics of Ice* (Oxford University Press, New York, 1999), 373 pp.
W.A. Phillips, Tunnelling states in amorphous solids. Bull. Am. Phys. Soc. **17**(1), 115 (1972)
P. Picker, E. Tremblay, C. Jolicoeur, Heat capacity measurements of liquids with a Picker mixing flow microcalorimeter. J. Solut. Chem. **3**, 377 (1974)
D. Prialnik, J. Benkhoff, M. Podolak, Modeling the structure and activity of comet nuclei. Comets **II**, 359–387 (2004)
F. Postberg, S. Kempf, J. Schmidt, N. Brilliantov, A. Beinsen, B. Abel, U. Buck, R. Srama, Sodium salts in E-ring ice grains from an ocean below the surface of Enceladus. Nature **459**, 1098–1101 (2009)
O. Prieto-Ballesteros, J.S. Kargel, Thermal state and complex geology of a heterogeneous salty crust of Jupiter's satellite Europa. Icarus **173**, 212–221 (2005)
R. Raj, M.F. Ashby, On grain boundary sliding and diffusional creep. Metall. Trans. **2**, 1113–1127 (1971)
R.O. Ramseier, Self-diffusion in ice monocrystals. US Army Cold Regions Research and Engineering Laboratory Hanover, NH, Research Report, 232 (1967a)
R.O. Ramseier, Self-diffusion of tritium in natural and synthetic ice monocrystals. J. Appl. Phys. **38**, 2553–2556 (1967b)
M. Randall, F.D. Rossini, Heat capacities in aqueous salt solutions. J. Am. Chem. Soc. **51**, 323–345 (1929)
M. Randall, M.D. Taylor, Heat capacity and density of aqueous solutions of potassium iodate, potassium acid sulfate, iodic acid, and sulfuric acid at 25 degrees C. J. Phys. Chem. **45**(6), 959–967 (1941)
J.H. Roberts, F. Nimmo, Tidal heating and the long-term stability of a subsurface ocean on Enceladus. Icarus **194**, 675–689 (2008)

E.J. Rosenbaum, N.J.K. English Johnson, D.W. Shaw, R.P. Warzinski, Thermal conductivity of methane hydrate from experiment and molecular simulation. J. Phys. Chem. B **111**(46), 13194–13205 (2007)
R.G. Ross, J.S. Kargel, Thermal conductivity of solar system ices, with special reference to Martian polar caps, in *Solar System Ices*, ed. by C. de Bergh, M. Festou, B. Schmitt (Kluwer, Dordrecht, 1998), pp. 33–62
R.G. Ross, P. Andersson, G. Backstrom, Effects of h-order and d-order on thermal-conductivity of ice phases. J. Chem. Phys. **68**(9), 3967–3972 (1978)
R.G. Ross, P. Andersson, G. Backstrom, Unusual pt dependence of thermal-conductivity for a clathrate hydrate. Nature **290**(5804), 322–323 (1981)
K. Seiferlin, T. Spohn, J. Benkhoff, Cometary ice texture and the thermal revolution of comets. Lab. Planetol. **15**(10), 35–38 (1995)
K. Seiferlin, N. I Komle, G. Kargl, Line heat-source measurements of the thermal conductivity of porous H2O ice, CO2 ice and mineral powders under. Planet. Space Sci. **44**(7), 691–704 (1996)
N.M. Schneider, M.H. Burger, E.L. Schaller, M.E. Brown, R.E. Johnson, J.S. Kargel, M. Dougherty, N. Achilleos, No sodium in Enceladus' vapor plumes. Nature **459**, 1102–1104 (2009)
E.M. Schulson, P. Duval, *Creep and Fracture of Ice* (Cambridge University Press, New York, 2009)
M.A. Simard, J.L. Fortier, Heat-capacity measurements of liquids with a picker mixing flow microcalorimeter source. Canadian J. of Chemistry-Revue Canadienne de Chimie **59**(22), 3208–3211 (1981)
G.A. Slack, Thermal conductivity of ice. Phys. Rev. B **22**, 3065–3071 (1980)
G. Steiner, N.I. Kömle, A model of the thermal-conductivity of porous water ice at low gas-pressures. Planet. Space Sci. **39**(3), 507–513 (1991)
L.A. Stern, W.B. Durham, S.H. Kirby, Grain-size-induced weakening of H_2O ices I and II and associated anisotropic recrystallization. J. Geophys. Res. **102**, 5313–5325 (1997)
E.R. Stofan et al., The lakes of Titan. Nature **445**, 61–64 (2007)
E. Tombari, S. Presto, G. Salvetti, G.P. Johari, Heat capacity of tetrahydrofuran clathrate hydrate and of its components, and the clathrate formation from supercooled melt. J. Chem. Phys. **124**(15), 154507 (2006)
S.H. Treagus, Viscous anisotropy of two-phase composites, and applications to rocks and structures. Tectonophysics **372**(3–4), 121–133 (2003)
J.S. Tse, M.A. White, Origin of glassy crystalline behaviour in thermal properties of clathrate hydrates: a thermal conductivity study of tetrahydrofuran hydrate. J. Phys. Chem. **92**, 5006–5011 (1988)
T.E. Tullis, F.G. Horowitz, J. Tullis, Flow laws of polyphase aggregates from end-member flow laws. J. Geophys. Res. **96**, 8081–8096 (1991)
G. Wakahama, On the plastic deformation of single crystal of ice, in *Proceedings of the International Conference on Low Temperature Science*, vol. 1 (Inst. of Low Temp. Sci., Hokkaido Univ., Sapporo, 1967), pp. 292–311
W.F. Waite, L.A. Stern, S.H. Kirby, W.J. Winters, D.H. Mason, Simultaneous determination of thermal conductivity, thermal diffusivity and specific heat in sI methane hydrate. Geophys. J. Int. **169**, 767–774 (2007)
J. Weertman, Dislocation climb theory of steady-state creep. Trans. ASM **61**, 681–694 (1968)
M.A. White, M.T. MacLean, Rotational freedom of guest molecules in tetrahydrofuran clathrate hydrate, as determined by heat capacity measurements. J. Phys. Chem. **89**, 1380–1383 (1985)
M.Yu. Zolotov, J.S. Kargel, Chemical composition of Europa's ice shell, ocean, and underlying rocks, in *Europa*, ed. by R. Pappalardo. Space Science (University of Arizona Press, Tucson, 2008, in press)